Hindawi
Security and Communication Networks
Volume 2022, Article ID 3923724, 16 pages
https://doi.org/10.1155/2022/3923724

Research Article

Secure Downlink Transmission in Cell-Free Massive MIMO System Enhanced by Intelligent Reflecting Surfaces

Huazhi Hu,[1] **Wei Xie**,[1] **Kui Xu**,[1] **Xiaochen Xia**,[1] **Meng Wang**,[1] **Shengwei Liu**,[2] **and Na Li**[1]

[1]*Army Engineering University of PLA, Nanjing 210007, China*
[2]*Unit 31401 of PLA, Jinan 250002, China*

Correspondence should be addressed to Wei Xie; edifier77@163.com

Received 4 March 2022; Accepted 11 May 2022; Published 13 July 2022

Academic Editor: Mohammad Ayoub Khan

This paper presents the application of intelligent reflecting surfaces (IRSs) in a cell-free massive MIMO network to enhance secure transmission in the system. Multiantenna access points (APs) need to transmit information to users safely and reliably via IRSs without fully knowing the channel state information (CSI) of a multiantenna eavesdropper (Eve) or the accurate beamforming information of a jammer. Specifically, through joint optimization of the AP active beamforming (ABF) and IRS passive beamforming (PBF), the information leaked to the Eve is limited by a set threshold, and restrictions on the IRS reflection phase are considered to maximize the weighted sum rate of the system's downlink transmission. To solve this multivariate-coupled nonconvex problem, we propose a joint precoding framework under imperfect CSI, using the generalized S-procedure, fractional programming (FP), and multidimensional complex quadratic transformation (MCQT) to transform the original complex nonconvex problem into an easily solvable convex optimization problem, and an alternating algorithm to obtain the optimal solution for precoding and IRS phase shifting. Simulation results show that the proposed scheme can significantly increase the weighted sum rate of the system compared to conventional antijamming methods while revealing that the scheme is effective in enhancing secure system transmission.

1. Introduction

Massive multiple-input multiple-output (MIMO) communication has been an extremely active research area in the field of wireless communication in recent years. As a key technology for fifth-generation (5G) networking, massive MIMO is allocated more antennas than conditional MIMO. It can tap deeply into the available wireless resources in the spatial dimension and use this spatial diversity to serve user terminals via the same time-frequency resources. Then, massive MIMO achieves the advantages of high spectrum/power efficiency and strong anti-interference capabilities [1–3]. Cell-free massive MIMO reverses the situation by deployed many access points (APs) with several antennas. By multi-AP collaboration and an improved signal-to-noise ratio (SNR) with the coherent transmission, cell-free massive MIMO improves user quality fairness [4, 5].

Intelligent reflecting surfaces (IRSs) are also known as reconfigurable intelligent surfaces (RISs) [6] or software-controlled metasurfaces [7]. It has emerged as an important approach for 5 G/6 G wireless communication systems to achieve intelligence in wireless channel/propagation environments. In general, an IRS consists of an intelligent controller and a passive reflector array, usually in a linear or planar configuration. The intelligent controller is connected to a BS or AP and controls the adjustment of the reflector array in real time. A large number of subwavelength-structured low-cost elements form a passive reflector array, which can independently induce controlled changes in the amplitude and/or phase of the incident signal with very low energy consumption [8]. Under the control of the intelligent controller, the reflected signals are coherently superimposed in the desired direction to achieve beamforming [9]. Unlike in traditional MIMO relaying, an IRS is not equipped with signal sensing elements and does not have signal reception

or processing capabilities. An IRS consumes very little energy and introduces no additional thermal noise during the passive reflection of the signal, which gives it significant energy and cost advantages over conventional repeaters [10].

The combination of cell-free massive MIMO and IRS technology to build reconfigurable wireless communication environments is emerging as a popular topic of research. Single-user communication in cell-free massive MIMO assisted by a single aerial IRS (AIRS) was studied in [11]; the authors of [12] considered a multiuser scenario and maximized the sum rate of all users; to obtain cooperative gains from multi-AP coherent transmission, the authors of [13] considered multiple-IRS-assisted single-user communication; and the use of multiple IRSs in multi-AP communication with multiple cell users was considered in [14] to assist in obtaining the maximum sum rate. In addition, scholars have investigated minimizing the transmission power in IRS-assisted massive MIMO communication scenarios [15], maximizing the energy efficiency [6], and maximizing the minimum SNR based on IRSs considering the fairness of user communication quality [16]. The authors of [17] studied the joint design of BS and IRS precoding frameworks in IRS-assisted cell-free massive MIMO to improve network capacity with low cost and low energy consumption of the IRSs.

1.1. Previous Works. Secure transmission has always been an integral part of wireless communication networks. The authors of [18] were the first to investigate the effect of a combined BS data precoding and artificial noise (AN) precoding strategy on the achievable secrecy rate of system communication in a collaborative/noncollaborative multicell massive MIMO scenario. The authors of [19] considered the performance of massive MIMO in resisting eavesdropping under impaired hardware and incomplete channel state information (CSI). However, research on the security of the physical layer in cell-free massive MIMO is still in its infancy. The authors of [20] investigated the security of multiantenna transmitters communicating with single-antenna receivers, jointly optimizing the beamforming of the transmitters and IRS phase shifting to maximize the secrecy of the system in a scenario with malicious eavesdropping by eavesdropper (Eve). Secure transmission in IRS-assisted MIMO was studied in [21]. Specifically, the authors introduced IRS into massive MIMO and designed AN to degrade the reception performance of an Eav, jointly designing the BS active precoding, AN interference, and IRS passive beamforming to improve the system secrecy despite transmission power constraints.

Furthermore, the authors of [22] considered secure communication in an IRS-assisted massive MIMO system. They assumed that the BS has access to incomplete CSI from third-party nodes and does not know the transmit beam formation of the jammer, and attempted to limit the information leakage to potential Eavs as much as possible. The aim is to maximize the system achievable rate by jointly designing the active precoding of the BS and the reflected phase shift of the IRS. The authors of [23] studied a secure transmission method in the presence of an active Eav in a cell-free massive MIMO system. They proposed a spatial-domain beamforming method based on channels with nonoverlapping arrival angles of the Eve and legitimate users to obtain the downlink transmission secrecy rate in a multipath channel model. The secrecy rate of cell-free MIMO in active attack scenarios based on the spatially correlated Rayleigh channel model was studied in [24]. The authors of [25] studied the secrecy rate of downlink transmission in an energy recovery scenario. The authors compared the secrecy of centralized massive MIMO and cell-free massive MIMO systems and proposed a power optimization scheme based on semidefinite relaxation planning based on derivations of the energy recovery and ergodic secrecy rate of an active Eve. The authors of [26] considered the secrecy rate problem for cell-free massive MIMO systems in the presence of pilot spoofing attacks, proposed a mechanism for detecting pilot spoofing attacks based on the minimum description length, and evaluated the secrecy performance of the system using the traversal secrecy rate. The authors of [27] proposed the use of an IRS to enhance the secrecy of a cell-free massive MIMO system in an experimental pilot spoofing attack scenario. By optimizing the transmit power coefficient of the AP and the IRS phase shift to design a secure and robust downlink transmission scheme. They minimized the information stolen by the Eve and ensured the quality of service for legitimate users. Moreover, [28] proposed the IRS can be utilized to suppress the information leakage towards malicious terminals. The authors jointly designed downlink beamformers and IRS phase shifts to improve the secrecy gain.

1.2. Contributions. The existing literature has considered only the presence of single-antenna jammer and single-antenna Eve in conventional massive MIMO. But there is still room for further research on secure transmission in cell-free massive MIMO scenarios, in which APs are deployed more extensively. Therefore, this paper considers the presence of a multiantenna jammer and a multiantenna Eve in a cell-free massive MIMO network. We construct a joint optimization framework to improve the weighted sum rate of the system, with the following main contributions.

(i) The current literature considers only the antijamming and eavesdropping performance of traditional MIMO systems. In this paper, we consider the use of IRSs to antijamming and eavesdropping. First, a novel secure transmission framework for an IRS assisted cell-free MIMO system with a multiantenna jammer and an Eve is proposed.

(ii) We jointly optimize the ABF and PBF to improve the sum rate. The central processing unit (CPU) is not fully aware of the CSI of the Eve or the beamforming information of the jammer. Specifically, considering the CSI error, a joint precoding framework is designed to limit the information leaked to the Eve while considering an IRS phase constraint and maximizing the weighted sum rate.

(iii) The coupling of multiple variables and multiple constraints makes the solution of nonconvex problems more difficult. To overcome this challenge, we first use the generalized S-procedure to convert the constraints into a manageable mathematical form. Then, we design a framework for joint optimization under imperfect CSI and transform the original problem into a solvable nonconvex optimization. During this process, auxiliary variables are introduced and using mathematical transformations such as fractional programming (FP) and multidimensional complex quadratic transformation (MCQT). Finally, we obtain the optimal solution using an alternating algorithm.

(iv) Our proposed scheme is compared with conventional antijamming and eavesdropping methods through simulation experiments, and the experimental results demonstrate the effectiveness of our proposed secure transmission scheme for an IRS-assisted cell-free massive MIMO system.

1.3. Organization and Notation. Organization: The main structure of this paper is as follows. The system model for IRS-assisted cell-free massive MIMO multiuser secure transmission is presented in Section 2. In Section 3, we describe the problem and propose an objective function for optimization. In Section 4, we present a joint precoding framework for maximizing the sum rate of the system in an imperfect CSI scenario. The results of simulation experiments are presented in Section 5 to verify the performance of the proposed IRS-assisted cell-free massive MIMO system in resisting jamming and eavesdropping. Finally, conclusion is drawn in Section 6.

Notation: Throughout this paper, bold capital and lowercase letters denote matrices and vectors, respectively. $[\cdot]^*$, $[\cdot]^{-1}$, $[\cdot]^T$, and $[\cdot]^H$ denote the conjugate, inverse, transpose, and conjugate transpose operations, respectively. $\mathbb{C}^{M\times N}$ represents the set of all $M \times N$ complex-valued matrices. $\mathbb{N}^{m\times m}$ denotes the set of all $m \times m$ Hermitian matrices. $\mathbb{R}$ denotes the set of real numbers. $\mathbf{A} \succ 0$ indicates that $\mathbf{A}$ is a positive semidefinite matrix. $\det(\mathbf{A})$ and $\|\mathbf{A}\|_F$ represent the determinant and Frobenius norm, respectively, of matrix $\mathbf{A}$. $E[\cdot]$ is the expectation operator, and $\mathrm{diag}(\cdot)$ represents the diagonal operation. $\mathbf{I}_L$ denotes the $L \times L$ identity matrix, and e_l is an elementary vector with a 1 in the l-th position. 1_L denotes a column vector of length L with all elements equal to 1. $\otimes$ denotes the Kronecker product.

2. System Model

2.1. Channel Model. As shown in Figure 1, we consider secure transmission in an IRS-assisted cell-free massive MIMO system, where M multiantenna APs communicate with K multiantenna users with the assistance of an IRS. When a multiantenna jammer and a multiantenna Eve are present on the downlink, the jammer attempts to interfere by transmitting jamming signals through the direct link with a user and the jammer–IRS–user cascade channel, and the Eve attempts to steal legally transmitted information through the AP–IRS–Eve cascade channel and the direct channel. Specifically, each AP is equipped with L antennas, each user and the Eve have U antennas, and the independent jammer is also equipped with Q antennas, while the IRS is composed of N reflective primitives. The CPU is connected to the APs and the IRS via a perfect forward link. The CPU maximizes the sum rate of the system by adjusting the active precoding vector of the APs and the reflected phase shift of the IRS in real time to resist malicious interference from the jammer and reduce the information leaked to the Eve.

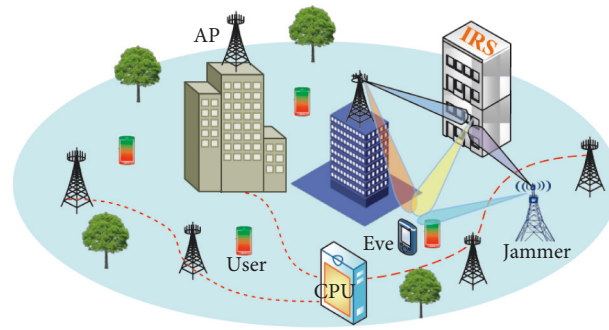

Figure 1: Schematic diagram of IRS-assisted communication.

As shown in Figure 2, there are two types of communication links between an AP and a user: the first is a direct AP/jammer–user link, and the second is an AP–IRS–user cascade link. Similarly, there are direct links and cascade links between the jammer and a user. Due to the severe signal loss incurred in multihop reflections [29], the effect of only one reflection in a cascade link is considered in this paper. For the cell-free massive MIMO scenario, the previous literature has usually assumed that the CPU perfectly knows the CSI of a channel; however, it is usually difficult for the CPU to obtain perfect CSI for each channel due to the high density of AP deployment and the fact that the IRS is almost passive and cannot perform any signal processing. Therefore, we consider the system performance of an IRS-assisted cell-free massive MIMO system in resisting jamming and eavesdropping in the case in which the CPU cannot obtain perfect CSI of the jammer or Eve.

The equivalent channel between the m-th AP and the k-th legitimate user/Eve can be represented as

$$\mathbf{F}_{m,i}^H = \mathbf{H}_{m,i}^H + \mathbf{R}_i^H \Theta^H \mathbf{G}_m i \in \{1, 2, \ldots, M, Eve\}, \quad (1)$$

where $\mathbf{H}_{m,i} \in \mathbb{C}^{L\times U}$ denotes the direct channel link between the m-th AP and the i-th legitimate user/Eve, $\mathbf{R}_i^H \Theta^H \mathbf{G}_m \in \mathbb{C}^{U\times L}$ denotes the cascade channel between the m-th AP and the i-th legitimate user/Eve, $\mathbf{R}_i \in \mathbb{C}^{N\times U}$ denotes the channel from the IRS to the i-th legitimate user/Eve, $\mathbf{G}_m \in \mathbb{C}^{N\times L}$ denotes the channel between the m-th AP and the IRS, and $\Theta \in \mathbb{C}^{N\times N}$ represents the phase shift matrix of the IRS. Specifically, $\Theta = \sqrt{\eta}\mathrm{diag}([\theta_1, \theta_2, \ldots, \theta_N]^T)$, where η is the IRS reflection coefficient. In practice, efforts have been made to study the effects of both the reflection amplitude and reflection phase of the IRS on the system [30]. In this paper, only the effect of the IRS reflection phase is considered, and for illustrative purposes, we set the reflection

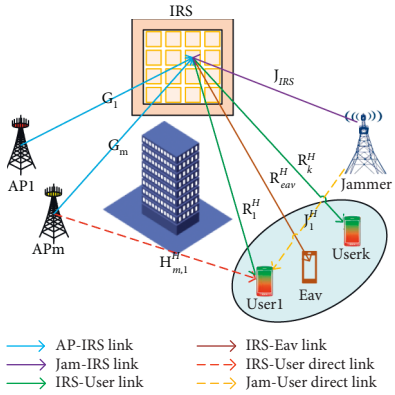

FIGURE 2: IRS-assisted cell-free massive MIMO antijamming and eavesdropping.

coefficient to 1. θ_n is the phase of the n-th reflective element of the IRS and can be written as

$$\theta_n \in \Omega, \Omega = \left\{\theta_n = e^{j\varphi_n} \middle| |\theta_n|^2 < 1, \varphi_n \in [0, 2\pi)\right\}. \tag{2}$$

Between the jammer and a user, we consider a direct link and a primary reflected jammer–IRS–user cascade link, for which the equivalent channel can be expressed as

$$\mathbf{B}_i^H = \mathbf{J}_i^H + \mathbf{R}_i^H \Theta^H \mathbf{J}_{IRS}, i \in \{1, 2, \ldots, M, Eve\}, \tag{3}$$

where $\mathbf{J}_i \in \mathbb{C}^{Q\times U}$ denotes the direct channel between the jammer and the k-th user/Eve, $\mathbf{R}_k^H \Theta^H \mathbf{J}_{IRS} \in \mathbb{C}^{U\times Q}$ represents the cascade channel between the jammer and the k-th user/Eve, and $\mathbf{J}_{IRS} \in \mathbb{C}^{N\times Q}$ represents the channel from the jammer to the IRS.

For secure transmission in IRS-assisted massive MIMO scenarios, previous studies have typically assumed that an AP can accurately acquire an Eve's CSI. Legitimate users perform channel estimation by sending guide signals to the APs, so the APs can periodically obtain the CSI of legitimate users. However, Eve does not reflect signals to the APs and usually hide their presence from the APs, so it is not feasible to obtain accurate CSI through cooperation between an Eve and an AP. Similarly, the CSI between a jammer and a user is also difficult to obtain. It has been proposed in the literature [31] that channel estimation can be performed using signals leaked from an Eve to an AP, but the error in the CSI collected via this approach is both too large and outdated. To study the system performance, such as the AP–IRS–Eve and jammer–IRS–user performance, in the case of imperfect CSI, a deterministic model is used in this paper to describe the uncertainty of the CSI [32–35], and the CSI between an AP and the Eve is modelled as follows:

$$\mathbf{F}_{m,Eve} = \overline{\mathbf{F}}_{m,Eve} + \Delta\mathbf{F}_{m,Eve}, \left\|\Delta\mathbf{F}_{m,Eve}\right\|_F \leqslant \varepsilon_{m,Eve}, \tag{4}$$

$$\mathbf{J}_i = \overline{\mathbf{J}}_i + \Delta\mathbf{J}_i, \left\|\Delta\mathbf{J}_i\right\|_F \leqslant \varepsilon_{j,i}, \tag{5}$$

where $\overline{\mathbf{F}}_{m,Eve} \in \mathbb{C}^{L\times U}$ denotes the estimated channel between the m-th AP and the Eve, $\overline{\mathbf{J}}_i \in \mathbb{C}^{Q\times U}$ denotes the estimated channel for the direct link between the jammer and the i-th user, and $\Delta\mathbf{F}_{m,Eve}$ and $\Delta\mathbf{J}_{IRS}$ denote the corresponding estimation errors for each channel. $\varepsilon_{m,Eve}$ and $\varepsilon_{j,i}$ denote the uncertainty radii of the individual estimation errors, which represent the level of uncertainty and are usually set relatively small for more accurate quantization and channel estimation algorithms. Equations (4) and (5) employ a flexible and general CSI uncertainty model [36], which is able to represent the bounded CSI uncertainty when attempting to obtain accurate CSI in IRS-assisted cell-free massive MIMO systems due to the influence of individual error factors.

2.2. Transmitters and Jammer. To obtain the cooperative benefits of coherent transmission from multi-AP collaboration, all APs in the IRS-assisted cell-free massive MIMO system proposed in this paper are synchronized to serve all users in the area through coherent joint transmission [37]. In the downlink direction, the signal transmitted by the m-th AP can be expressed as

$$\mathbf{s}_m = \sum_{k=1}^{K} \mathbf{w}_{m,k} x_k, \tag{6}$$

where x_k denotes the data signal transmitted to the k-th user, and we assume that the normalized power of this signal is $\mathrm{E}[|x_k|^2] = 1$, while $\mathbf{w}_{m,k} \in \mathbb{C}^L$ represents the precoding vector of the m-th AP for the k-th user. Similarly, the jammer expects to send a scrambled jamming signal to the user, which can be expressed as

$$\mathbf{j} = \sum_{k=1}^{K} \mathbf{v}_k m_k, \tag{7}$$

where m_k represents the jamming signal sent by the jammer to the k-th user, with $\mathrm{E}[|m_k|^2] = 1$, and $\mathbf{v}_k \in \mathbb{C}^Q$ denotes the precoding vector of the jammer for the k-th user. According to [22], the precoding vector $\mathbf{v}$ of the jammer corresponds to zero-forcing (ZF) precoding. For multiantenna jammers, ZF precoding can effectively eliminate self-interference with little processing complexity, which is a conventional empirical assumption.

2.3. Legitimate Users and Eve. From the above, the received signal of the k-th user can be expressed as

$$\begin{aligned}\mathbf{y}_k = \sum_{m=1}^{M} \mathbf{F}_{m,k}^H \mathbf{s}_m + \mathbf{B}_k^H \mathbf{j} + \mathbf{z}_k = \sum_{m=1}^{M} \left(\mathbf{H}_{m,k}^H + \mathbf{R}_k^H \Theta^H \mathbf{G}_m\right) \mathbf{w}_{m,k} x_k \\ + \sum_{m=1}^{M} \sum_{b=1, b\neq k}^{K} \left(\mathbf{H}_{m,k}^H + \mathbf{R}_k^H \Theta^H \mathbf{G}_m\right) \mathbf{w}_{m,b} x_b \\ + \left(\mathbf{J}_k^H + \mathbf{R}_k^H \Theta^H \mathbf{J}_{IRS}\right) \mathbf{v}_k m_k + \mathbf{z}_k.\end{aligned} \tag{8}$$

The M APs serve all users simultaneously, so the information received by each user is a superposition of the information sent by all APs and the jamming information emitted by the jammer. In the above equation, the first term on the right-hand side is the signal that user k expects to receive, and the next three terms are the information sent by

the AP to other users, the information sent by the jammer and the noise.

$$\mathbf{y}_{Eve} = \sum_{m=1}^{M} \mathbf{F}_{m,Eve}^{H}\mathbf{s}_m + \mathbf{B}_{Eve}^{H}\mathbf{j} + \mathbf{z}_{Eve}, \tag{9}$$

$\mathbf{z}_i$, $i \in \{1, 2, \ldots, M, Eve\}$, denotes Gaussian white noise with mean 0 and variance $\Xi_i = \sigma_i^2\mathbf{I}_U$ for the i-th legitimate user/Eve.

3. Problem Formulation

Based on the above system model, in this section, we consider the weighted sum rate of the IRS-assisted cell-free massive MIMO antijamming and eavesdropping system under imperfect CSI, satisfying constraints on the AP transmit power, the IRS reflection phase, and the Eve's maximum information rate.

We define $\mathbf{F}_k = [\mathbf{F}_{1,k}^T, \mathbf{F}_{2,k}^T, \ldots, \mathbf{F}_{M,k}^T]^T$ and $\mathbf{w}_k = [\mathbf{w}_{1,k}^T, \mathbf{w}_{2,k}^T, \ldots, \mathbf{w}_{M,k}^T]^T$. By substituting equation (3) into (8), equation (8) can be rewritten as

$$\mathbf{y}_k = \sum_{m=1}^{M}\sum_{b=1}^{K} \mathbf{F}_{m,b}^{H}\mathbf{w}_{m,b}\mathbf{s}_m + \mathbf{B}_k^{H}\mathbf{j} + \mathbf{z}_k = \sum_{b=1}^{K} \mathbf{F}_k^{H}\mathbf{w}_b\mathbf{s}_b + \mathbf{B}_k^{H}\mathbf{j} + \mathbf{z}_k. \tag{10}$$

The signal-to-interference-plus-noise ratio (SINR) of the received signal for the k-th user can be expressed as

$$r_k = \mathbf{w}_k^{H}\mathbf{F}_k\left[\sum_{b=1,b\neq k}^{K} \mathbf{F}_k^{H}\mathbf{w}_b\left(\mathbf{F}_k^{H}\mathbf{w}_b\right)^{H} + \mathbf{B}_k^{H}\mathbf{v}_k\left(\mathbf{B}_k^{H}\mathbf{v}_k\right)^{H} + \mathbf{\Gamma}_k\right]^{-1}\left(\mathbf{w}_k^{H}\mathbf{F}_k\right)^{H}. \tag{11}$$

Therefore, the weighted sum rate for all users can be written as

$$R_s = \sum_{k=1}^{K} \omega_k \log_2\left(1 + r_k\right), \tag{12}$$

where ω_k denotes the weighting factor for the k-th user. We define $\mathbf{F}_{Eve} = [\mathbf{F}_{1,Eve}^T, \mathbf{F}_{2,Eve}^T, \ldots, \mathbf{F}_{M,Eve}^T]^T$. Similarly, the signal received by the Eve can be written as

$$\mathbf{y}_{\text{Eve}} = \sum_{m=1}^{M}\sum_{b=1}^{K} \mathbf{F}_{m,\text{Eve}}^{H}\mathbf{w}_{m,b}\mathbf{s}_m + \mathbf{z}_{\text{Eve}} = \sum_{b=1}^{K} \mathbf{F}_{Eve}^{H}\mathbf{w}_b\mathbf{s}_b + \mathbf{z}_k. \tag{13}$$

The achievable rate of the Eve can be written as

$$R_{\text{Eve}}^{k} = \log_2\det\left(\mathbf{I}_U + \left(\sum_{b=1,b\neq k}^{K} \mathbf{F}_{\text{Eve}}^{H}\mathbf{w}_b\mathbf{w}_b^{H}\mathbf{F}_{\text{Eve}} + \sigma_{\text{Eve}}^2\mathbf{I}_U\right)^{-1}\mathbf{F}_{\text{Eve}}^{H}\mathbf{w}_k\mathbf{w}_k^{H}\mathbf{F}_{\text{Eve}}\right). \tag{14}$$

We consider robust transmission under a bounded CSI uncertainty model. Let us define $\mathbf{W} = [\mathbf{w}_1^T, \mathbf{w}_2^T, \ldots, \mathbf{w}_k^T]^T$; then, the optimization problem for maximizing the weighted sum rate can be expressed as

$$\begin{aligned} P1:\ &\max_{W,\Theta} R_s(\mathbf{W}, \mathbf{\Theta}) = \sum_{k=1}^{K} \omega_k \log_2\left(1 + r_k\right), \\ &s.t.\ C1:\ R_{Eve}^{k} \le R_{th}, \\ &C2:\ \sum_{k=1}^{K} \left\|w_{m,k}\right\|^2 \le P_{m,\max}, \\ &C3:\ \theta_n \in \Omega, n = 1, 2, \ldots, N. \end{aligned} \tag{15}$$

where constraint C1 ensures secure transmission in the physical layer of the system and represents the upper limit on the rate at which an Eve can receive and the maximum level of information leakage that the system can tolerate from an Eve. Constraint C2 is the maximum transmit power limit per AP, and C3 represents the unit modulus constraint for the reflective elements of the IRS.

Remark 1. Equation (15) is a generalization of the optimization problem in the IRS-assisted cell-free massive MIMO antijamming and eavesdropping scenario. Under the three constraints, the objective function is not jointly convex in $\mathbf{W}$ and Θ, and there is multiple coupling among the variables. The nonclosed-form solution of constraint C1 and the highly nonconvex nature of constraint C3 make the optimization of the objective function a tricky problem. In the next section, we propose a joint precoding scheme under imperfect CSI to obtain an optimal solution.

4. Joint Precoding Design with Imperfect CSI

In this section, we derive in detail the procedure for solving problem P1. Specifically, in Section IV-A, the objective function is transformed into a manageable form by introducing variables. In Sections IV-B and IV-C, the nonconvex constraints C1 and C3 are treated mathematically with fixed IRS phase-shift matrices and AP active precoding, respectively, so that the problem becomes a solvable convex optimization problem, and an alternating optimization algorithm is proposed to solve for the optimal values.

4.1. Processing of the Objective Function. As in reference [38], we introduce auxiliary variables $\zeta \in \mathbb{R}^K$, $\zeta = [\zeta_1, \zeta_2, \ldots, \zeta_K]^T$, in order to rewrite equation (12) as

$$P2:\ \max_{W,\Theta,\zeta} R_s(\mathbf{W},\boldsymbol{\Theta},\boldsymbol{\zeta}) = \sum_{k=1}^{K}\left[\omega_k \log_2(1+\zeta_k) - \omega_k\zeta_k + \frac{\zeta_k(1+\omega_k)r_k}{1+r_k}\right] s.t.\ C1:\ R_{Eve}^{k} \le R_{th}; C2; C3. \tag{16}$$

By substituting equation (11) into (16), P2 can be further rewritten as P3

$$\begin{aligned} P3:\ &\max_{\mathbf{W},\Theta,\boldsymbol{\zeta}} \psi(\mathbf{W},\boldsymbol{\Theta},\boldsymbol{\zeta}) \\ \text{s.t. } C1:\ &R_{\text{Eve}}^{k} \le R_{\text{th}}, C2, C3, \end{aligned} \tag{17}$$

$$\psi(\mathbf{W},\boldsymbol{\Theta},\boldsymbol{\zeta}) = \sum_{k=1}^{K}\left[\omega_k \log_2(1+\zeta_k) - \omega_k\zeta_k + \zeta_k(1+\omega_k)\psi_k(\mathbf{W},\boldsymbol{\Theta})\right], \tag{18}$$

$$\psi_k(\mathbf{W},\boldsymbol{\Theta}) = \mathbf{w}_k^H\mathbf{F}_k\left[\sum_{b=1}^{K}\mathbf{F}_k^H\mathbf{w}_b\left(\mathbf{F}_k^H\mathbf{w}_b\right)^H + \mathbf{B}_k^H\mathbf{v}_k\left(\mathbf{B}_k^H\mathbf{v}_k\right)^H\boldsymbol{\Gamma}_k\right]^{-1}\left(\mathbf{w}_k^H\mathbf{F}_k\right)^H. \tag{19}$$

Given $\mathbf{W}$ and Θ, the optimal ζ can be found from $\partial\psi/\partial\zeta_k = 0$, k $= 1, 2, \ldots,$ K:

$$\zeta_k^{opt} = r_k^*, k = 1, 2, \ldots, K. \tag{20}$$

By substituting equation (20) into (16), it becomes possible to express the optimization problem only in terms of $\omega_k(1+\zeta_k^*)\psi_k(\mathbf{W},\Theta)$. Given ζ_k^*, P3 can be further rewritten as

$$\begin{aligned} P4:\ &\max_{W,\Theta,\zeta}\sum_{k=1}^{K}\omega_k(1+\zeta_k^*)\psi_k(\mathbf{W},\boldsymbol{\Theta}), \\ &\text{s.t. } C1:\ R_{\text{Eve}}^{k} \le R_{\text{th}}; C2; C3. \end{aligned} \tag{21}$$

The nonclosed-form solution for constraint C1 presents a major difficulty in solving P4. To solve this problem, we transform C1 into a manageable equivalent form as described in the following proposition and lemma.

Proposition 1. *Constraint C1 has the following equivalent representation (The derivation is described in Appendix):*

$$C1 \Leftrightarrow \mathbf{F}_{\text{Eve}}^H\left[\left(2^{R_{\text{th}}}-1\right)\sum_{b=1,b\neq k}^{K}\mathbf{w}_b\mathbf{w}_b^H - \mathbf{w}_k\mathbf{w}_k^H\right]\mathbf{F}_{\text{Eve}} + \left(2^{R_{\text{th}}}-1\right)\sigma_{\text{Eve}}^2\mathbf{I}_U \succcurlyeq 0. \tag{22}$$

Proof. Please refer to Appendix.

The initial transformation of constraint C1 is given by Proposition 1, but the solution process still has a high degree of complexity. There are several effective ways to address the inequality constraint C1; in this paper, constraint C1 will be further treated using the approach of the generalized S-procedure, as described in Lemma 1 [39]. □

Lemma 1. *Consider the following quadratic matrix inequality (generalized S-procedure):*

$$\begin{aligned} &f(\mathbf{Y}) = \mathbf{Y}^H\mathbf{B}\mathbf{Y} + \mathbf{Y}^H\mathbf{C} + \mathbf{C}^H\mathbf{Y} + \mathbf{D} \succcurlyeq 0, \\ &\forall\mathbf{Y} \in \left\{\mathbf{S} | Tr\left(\mathbf{T}\mathbf{S}\mathbf{S}^H\right) \leqslant 1, \mathbf{T} \succcurlyeq 0\right\}, \end{aligned} \tag{23}$$

where $\mathbf{B}, \mathbf{T} \in \mathbb{N}^m$, $\mathbf{Y}, \mathbf{C} \in \mathbb{C}^{m\times n}$, *and* $\mathbf{D} \in \mathbb{N}^n$. *The quadratic matrix inequality exists when and only when* $\mu > 0$.

$$\begin{bmatrix} \mathbf{D} & \mathbf{C}^H \\ \mathbf{C} & \mathbf{B} \end{bmatrix} - \mu\begin{bmatrix} \mathbf{I}_n & 0 \\ 0 & -\mathbf{T} \end{bmatrix} \succcurlyeq 0. \tag{24}$$

Consider equation (5) and the definition

$$\mathbf{F}_{\text{Eve}} = \overline{\mathbf{F}}_{\text{Eve}} + \Delta\mathbf{F}_{\text{Eve}}, \tag{25}$$

where $\overline{\mathbf{F}}_{\text{Eve}} = [\overline{\mathbf{F}}_{1,\text{Eve}}^T, \overline{\mathbf{F}}_{2,\text{Eve}}^T, \ldots, \overline{\mathbf{F}}_{M,\text{Eve}}^T]$ and $\Delta\mathbf{F}_{Eve} = [\Delta\mathbf{F}_{1,\text{Eve}}^T, \Delta\mathbf{F}_{2,\text{Eve}}^T, \ldots, \Delta\mathbf{F}_{M,\text{Eve}}^T]$. By substituting equation (25) into (22), constraint C1 can be transformed into

$$\Delta\mathbf{F}_{\text{Eve}}^H\Gamma\Delta\mathbf{F}_{\text{Eve}} + \overline{\mathbf{F}}_{\text{Eve}}^H\Gamma\Delta\mathbf{F}_{\text{Eve}} + \Delta\mathbf{F}_{\text{Eve}}^H\Gamma\overline{\mathbf{F}}_{\text{Eve}} + \overline{\mathbf{F}}_{\text{Eve}}^H\Gamma\overline{\mathbf{F}}_{\text{Eve}} + \left(2^{R_{\text{th}}} - 1\right)\sigma_{\text{Eve}}^2\mathbf{I}_U \succcurlyeq 0 \Delta\mathbf{F}_{\text{Eve}}^H \in \left\{\mathbf{S} | Tr\left(\varepsilon_{\text{Eve}}^{-2}\mathbf{S}\mathbf{S}^H\right) \le 1\right\}, \tag{26}$$

where $\Gamma \triangleq (2^{R_{th}} - 1)\sum_{b=1,b\neq k}^{K}\mathbf{w}_b\mathbf{w}_b^H - \mathbf{w}_k\mathbf{w}_k^H$. With Lemma 1, constraint C1 can be written as

$$C1 \Leftrightarrow C1\prime\colon \mathbf{A} + \mathbf{P}\Gamma\mathbf{P}^H \succcurlyeq 0, \tag{27}$$

$$\mathbf{A} = \begin{bmatrix} \left[\left(2^{R_{th}} - 1\right)\sigma_{Eve}^2 - \mu\right]\mathbf{I}_U & 0 \\ 0 & \mu\mathbf{I}_{ML} \end{bmatrix}, \tag{28}$$

where $\mathbf{P} = [\overline{\mathbf{F}}_{Eve}^H\mathbf{I}_{ML}]^T$. After transformation, $\mathbf{A}$ is a simpler form of a linear matrix inequality, which is more suitable for algorithm design. The optimization problem P4 can therefore be further rewritten as

$$\text{P4:}\ \max_{\mathbf{W},\Theta,\zeta}\ \omega_k\left(1 + \zeta_k^*\right)\psi_k(\mathbf{W},\Theta) s.t. C1\prime\colon \mathbf{A} + \mathbf{P}\Gamma\mathbf{P}^H \succcurlyeq 0; \quad C2; C3. \tag{29}$$

At this point, we have completed the C1 transformation, and we will now design the active and passive precoding processes separately.

4.2. Active Precoding: Fix (Θ^*, ζ^*) and Solve for $\mathbf{W}^*$. By fixing (Θ^*, ζ^*), the problem of solving for $\mathbf{W}^*$ can be written as

$$P5\text{:}\ \max_{\mathbf{W}} f(\mathbf{W}) = \omega_k\left(1 + \zeta_k^*\right)\psi_k(\mathbf{W},\Theta^*) s.t. C1\prime\colon \mathbf{A} + \mathbf{P}\Gamma\mathbf{P}^H \succcurlyeq 0 \quad C2\text{:}\ \sum_{k=1}^{K}\left\|\mathbf{w}_{m,k}\right\|^2 \leqslant P_{m,\max}. \tag{30}$$

For the high-dimensional nonconvex objective function in problem P5, we use MCQT [38] to address the nonconvexity of the high-dimensional fraction; see Proposition 2.

Proposition 2. *With the introduction of auxiliary variables $\eta = [\eta_1, \eta_2, \ldots, \eta_K]$, $\eta_k \in \mathbb{C}^U$, with FP and MCQT, P5 can be further rewritten as*

$$P6\text{:}\ \max_{\mathbf{W},\boldsymbol{\eta}} f_1(\mathbf{W},\boldsymbol{\eta}) s.t. C1', C2, \tag{31}$$

where $f_1(\mathbf{W},\eta)$ can be specifically expressed as

$$f_1(\mathbf{W},\boldsymbol{\eta}) = \sum_{k=1}^{K} 2\sqrt{\omega_k\left(1 + \zeta_k^*\right)}\Re\left\{\boldsymbol{\eta}_k^H\mathbf{F}_k^H\mathbf{w}_k\right\}, - \sum_{k=1}^{K}\boldsymbol{\eta}_k^H\left(\sum_{b=1}^{K}\mathbf{F}_k^H\mathbf{w}_b\left(\mathbf{F}_k^H\mathbf{w}_b\right)^H + \mathbf{B}_k^H\mathbf{v}_k\left(\mathbf{B}_k^H\mathbf{v}_k\right)^H + \boldsymbol{\Gamma}_k\right)\boldsymbol{\eta}_k, \tag{32}$$

From equation (32), the optimal solution for $\mathbf{W}$ is obtained through the alternating optimization of η and $\mathbf{W}$ as follows. First, we fix $\mathbf{W}$ and solve for η^{opt}. We let $\partial f_1(\mathbf{W},\eta)/\partial\eta_k = 0$. Then, η_k^{opt} can be obtained from the following equation:

$$\boldsymbol{\eta}_k^{opt} = \sqrt{\omega_k\left(1 + \zeta_k^*\right)}\left(\sum_{b=1}^{K}\mathbf{F}_k^H\mathbf{w}_b\left(\mathbf{F}_k^H\mathbf{w}_b\right)^H + \mathbf{B}_k^H\mathbf{v}_k\left(\mathbf{B}_k^H\mathbf{v}_k\right)^H + \boldsymbol{\Gamma}_k\right)^{-1}\mathbf{F}_k^H\mathbf{w}_b, k = 1, 2, \ldots, K. \tag{33}$$

Then, we fix η and solve for $\mathbf{W}^{opt}$. For illustration, we define

$$\mathbf{d} = \sum_{k=1}^{K}\mathbf{F}_k\boldsymbol{\eta}_k\boldsymbol{\eta}_k^H\mathbf{F}_k^H, \tag{34}$$

$$\mathbf{D} = \mathbf{I}_K \otimes \mathbf{d}, \boldsymbol{\alpha}_k = \mathbf{F}_k\boldsymbol{\eta}_k, \mathbf{U} = \left[\boldsymbol{\alpha}_1^T, \boldsymbol{\alpha}_2^T, \ldots, \boldsymbol{\alpha}_K^T\right]^T. \tag{35}$$

By substituting equation (35) into (32), $f_1(\mathbf{W},\eta)$ in P6 can be written as

$$f_1(\mathbf{W}) = -\mathbf{W}\mathbf{D}\mathbf{W} + \Re\left\{2\mathbf{U}^H\mathbf{W}\right\}, - \sum_{k=1}^{K}\boldsymbol{\eta}_k^H\left(\mathbf{B}_k^H\mathbf{v}_k\left(\mathbf{B}_k^H\mathbf{v}_k\right)^H + \boldsymbol{\Gamma}_k\right)\boldsymbol{\eta}_k. \tag{36}$$

The third term in equation (37) is not related to $\mathbf{W}$. Thus, problem P6 can be written in a more concise form as

$$P7:\ \max_{\mathbf{W}} -\mathbf{WDW} + \Re\left\{2\mathbf{U}^H\mathbf{W}\right\},$$
$$s.t.\quad C1\prime:\ \mathbf{A} + \mathbf{P}\Gamma\mathbf{P}^H \succcurlyeq 0, \tag{37}$$
$$C2:\ \mathbf{W}^H\mathbf{MW} \leqslant P_{m,\max},$$

where $e \in \mathbb{R}^M$ and $\mathbf{M} = \mathbf{I}_K \otimes \{(ee^H) \otimes \mathbf{I}_L\}$. In equation (37), both $\mathbf{D}$ and $\mathbf{M}$ are semipositive definite; thus, they conform to the standard form of quadratically constrained quadratic programming and can be solved using a standard convex optimization toolbox.

4.3. Passive Precoding: Fix $(\mathbf{W}, \zeta)$ and Solve for Θ^{opt}. The problem of fixing $(\mathbf{W}, \zeta)$ and solving for the maximum weighted sum rate by optimizing the passive precoding scheme can be described as follows:

$$P8:\ \max_{\mathbf{\Theta}} f_2(\mathbf{\Theta}) = \sum_{k=1}^{K} \omega_k (1+\zeta_k^*)\psi_k(\mathbf{W}^*, \mathbf{\Theta}) s.t. C1\prime:\ \mathbf{A} + \mathbf{P}\Gamma\mathbf{P}^H \succcurlyeq 0 \quad C3:\ \theta_n \in \Omega, n = 1, 2, \ldots, N. \tag{38}$$

For illustration, we simplify $f_2(\Theta)$ in equation (38). First, we define

$$\mathbf{T}_{k,b}(\mathbf{\Theta}) \triangleq \sum_{m=1}^{M} \left(\mathbf{H}_{m.k}^H + \mathbf{R}_k^H \mathbf{\Theta}^H \mathbf{G}_m\right)\mathbf{w}_{m,b}. \tag{39}$$

By substituting equations (38) and (3) into equation (18), $f_2(\Theta)$ in problem P8 can be rewritten as

$$f_2(\mathbf{\Theta}) = \sqrt{\omega_k(1+\zeta_k^*)}\mathbf{T}_{k,k}^H(\mathbf{\Theta})\left[\sum_{b=1}^{K} \mathbf{T}_{k,b}(\mathbf{\Theta})\mathbf{T}_{k,b}^H(\mathbf{\Theta}) + \mathbf{B}_k^H\mathbf{v}_k\left(\mathbf{B}_k^H\mathbf{v}_k\right)^H + \mathbf{\Gamma}_k\right]^{-1}\mathbf{T}_{k,k}(\mathbf{\Theta}). \tag{40}$$

$f_2(\Theta)$ is still a high-dimensional fractional problem, and as before, we solve it using the method of MCQT in Proposition 2, with the procedure shown in Proposition 3.

Proposition 3. *We reintroduce the variables $\lambda = [\lambda_1, \lambda_2, \ldots, \lambda_K], \lambda_k \in \mathbb{C}^U$, and P8 can be rewritten as*

$$P9:\ \max_{\mathbf{\Theta}} f_3(\mathbf{\Theta}, \boldsymbol{\lambda}) = \sum_{k=1}^{K} \omega_k(1+\zeta_k^*)\overline{f}_3(\mathbf{\Theta}, \boldsymbol{\lambda}),$$
$$s.t.\quad C1', C3, \tag{41}$$

where $\overline{f}_3(\Theta, \lambda)$ can be expressed as

$$\overline{f}_3(\mathbf{\Theta}, \boldsymbol{\lambda}) = 2\sqrt{\omega_k(1+\zeta_k^*)}\Re\left\{\boldsymbol{\lambda}_k^H\mathbf{T}_{k,k}(\mathbf{\Theta})\right\}, - \boldsymbol{\lambda}_k^H\left(\sum_{b=1}^{K} \mathbf{T}_{k,b}(\mathbf{\Theta})\mathbf{T}_{k,b}^H(\mathbf{\Theta}) + \mathbf{B}_k^H\mathbf{v}_k\left(\mathbf{B}_k^H\mathbf{v}_k\right)^H + \mathbf{\Gamma}_k\right)\boldsymbol{\lambda}_k. \tag{42}$$

From equation (41), the process of solving for Θ^{opt} can be divided into two steps: first fixing Θ and solving for the locally optimal λ^{opt}, then fixing λ^{opt} and solving for the locally optimal Θ^{opt}. This alternating optimization process continues until convergence is reached.

First, we fix Θ and solve for λ^{opt}. Given Θ^*, we can obtain λ^{opt} from $\partial f_3(\Theta, \lambda)/\partial\lambda_k = 0$.

$$\boldsymbol{\lambda}_k^{opt} = \sqrt{\omega_k(1+\zeta_k^*)}\left(\sum_{b=1}^{K} \mathbf{T}_{k,b}(\mathbf{\Theta})\mathbf{T}_{k,b}^H(\mathbf{\Theta}) + \mathbf{B}_k^H\mathbf{v}_k\left(\mathbf{B}_k^H\mathbf{v}_k\right)^H + \mathbf{\Gamma}_k\right)^{-1}\mathbf{T}_{k,k}(\mathbf{\Theta}). \tag{43}$$

Then, we fix λ and solve for Θ^{opt}. Upon substituting λ^{opt} into equation (41), the solution for $f_3(\Theta, \lambda)$ in P9 has considerable complexity. We simplify the expression by first defining

$$\boldsymbol{\lambda}_k^H\mathbf{T}_{k,k}(\mathbf{\Theta}) \triangleq \sum_{m=1}^{M}\left(\boldsymbol{\lambda}_k^H\mathbf{H}_{m,k}^H\mathbf{w}_{m,b} + \boldsymbol{\lambda}_k^H\mathbf{R}_k^H\mathbf{\Theta}^H\mathbf{G}_m\mathbf{w}_{m,b}\right),$$
$$\triangleq \sum_{m=1}^{M}\boldsymbol{\lambda}_k^H\mathbf{H}_{m,k}^H\mathbf{w}_{m,b} + \tilde{\boldsymbol{\theta}}^H\sum_{m=1}^{M}\mathrm{diag}\left(\boldsymbol{\lambda}_k^H\mathbf{R}_k^H\right)\mathbf{G}_m\mathbf{w}_{m,b}, \tag{44}$$

where $\widetilde{\theta} = \Theta 1_N$.

For further simplification, we also define

$$h_{k,b} = \sum_{m=1}^{M} \boldsymbol{\lambda}_k^H \mathbf{H}_{m,k}^H \mathbf{w}_{m,b}, \mathbf{f}_{k,b} = \sum_{m=1}^{M} \operatorname{diag}\left(\boldsymbol{\lambda}_k^H \mathbf{R}_k^H\right) \mathbf{G}_m \mathbf{w}_{m,b}, \tag{45}$$

where $\mathbf{f}_{k,b} \in \mathbb{C}^N$. By substituting equation (45) into (44), equation (44) can be abbreviated as

$$\boldsymbol{\lambda}_k^H \mathbf{T}_{k,k}(\boldsymbol{\Theta}) = h_{k,b} + \widetilde{\boldsymbol{\theta}}^H \mathbf{f}_{k,b}, \tag{46}$$

$\overline{f}_3(\Theta, \lambda)$ can be written as

$$\begin{aligned} \overline{f}_3(\boldsymbol{\Theta}, \boldsymbol{\lambda}) = {} & 2\sqrt{\omega_k(1+\zeta_k^*)}\,\Re\left\{h_{k,k} + \widetilde{\boldsymbol{\theta}}^H \mathbf{f}_{k,k}\right\}, \\ & - \sum_{b=1}^{K}\left(h_{k,b} + \widetilde{\boldsymbol{\theta}}^H \mathbf{f}_{k,b}\right)\left(h_{k,b}^* + \mathbf{f}_{k,b}^H \widetilde{\boldsymbol{\theta}}\right), \\ & - \boldsymbol{\lambda}_k^H\left(\mathbf{B}_k^H \mathbf{v}_k \left(\mathbf{B}_k^H \mathbf{v}_k\right)^H + \boldsymbol{\Gamma}_k\right)\boldsymbol{\lambda}_k. \end{aligned} \tag{47}$$

We substitute equation (47) into P9, where $f_3(\Theta, \lambda)$ can be abbreviated to $f_4(\Theta, \lambda)$.

$$f_4(\boldsymbol{\Theta}, \boldsymbol{\lambda}) = -\widetilde{\boldsymbol{\theta}}^H \overline{\boldsymbol{\Lambda}} \widetilde{\boldsymbol{\theta}} + \Re\left\{2\widetilde{\boldsymbol{\theta}}^H \boldsymbol{\chi}\right\} + \beta, \tag{48}$$

$$\overline{\boldsymbol{\Lambda}} = \sum_{k=1}^{K} \sum_{b=1}^{K} \mathbf{f}_{k,b} \mathbf{f}_{k,b}^H, \tag{49}$$

$$\boldsymbol{\chi} = \sum_{k=1}^{K} \sqrt{\omega_k(1+\zeta_k^*)}\,\mathbf{f}_{k,k} - \sum_{k=1}^{K} \sum_{b=1}^{K} h_{k,b}^* \mathbf{f}_{k,b}, \tag{50}$$

$$\begin{aligned} \beta = {} & 2\sum_{k=1}^{K} \sqrt{\omega_k(1+\zeta_k^*)}\,\Re\left\{h_{k,k}\right\} - \sum_{k=1}^{K} \sum_{b=1}^{K} \left|h_{k,b}\right|^2, \\ & - \sum_{k=1}^{K} \boldsymbol{\lambda}_k^H\left(\mathbf{B}_k^H \mathbf{v}_k \left(\mathbf{B}_k^H \mathbf{v}_k\right)^H + \boldsymbol{\Gamma}_k\right)\boldsymbol{\lambda}_k. \end{aligned} \tag{51}$$

From (48), it follows that the optimization of Θ under a fixed λ is independent of the third term of (48). Therefore, P9 can be written in a more concise form as follows.

$$\begin{aligned} & P10: \min_{\boldsymbol{\Theta}} f_5(\boldsymbol{\Theta}) = \widetilde{\boldsymbol{\theta}}^H \overline{\boldsymbol{\Lambda}} \widetilde{\boldsymbol{\theta}} - \Re\left\{2\widetilde{\boldsymbol{\theta}}^H \boldsymbol{\chi}\right\}, \\ & s.t. \quad C1': \mathbf{A} + \mathbf{P}\boldsymbol{\Gamma}\mathbf{P}^H \succcurlyeq 0, \\ & C3: \quad \theta_n \in \Omega, n = 1, 2, \ldots, N. \end{aligned} \tag{52}$$

As the solution for the objective function in reference [40], $\overline{\Lambda}$ in P10 is a semipositive definite matrix, and the objective function is convex. Furthermore, it follows from the derivation of Proposition 1 and Equation (4) that the constraints C1′ and C3 are both convex, and the optimal solution for $\mathbf{A}$ can be obtained directly using the alternating direction method of multipliers (ADMM) [41] or the CVX toolbox. Finally, the proposed joint precoding algorithm is summarized in Algorithm 1.

5. Simulation Results

5.1. Simulation Setup. For the simulation setup in this paper, we refer to the deployment scenario of a cell-free massive MIMO network in [42] to construct the simulation scenario. Considering the mobility of the APs and IRS, our proposed algorithm supports stochasticity of the APs and IRS. In this paper, we use the 3D scene schematic shown in Figure 3 only as an example. In this cell-free massive MIMO network, 5 APs simultaneously serve 4 users in a given area, and there may be objects such as buildings and vegetation between the APs and the users. In this cell-free network, there are a malicious jammer and an Eve that attempt to jam and eavesdrop on legitimate users. To resist interference and eavesdropping, we deploy an IRS on a high building surface. Due to the high location of the IRS, an AP–IRS–user cascade link can be easily established to compensate for the high path loss on the direct link due to object occlusion and to resist

Input: All channels $\mathbf{H}_{m,i}$, $\mathbf{R}_i$, $\mathbf{G}_m$, $\mathbf{J}_i$ and $\mathbf{J}_{IRS}$; Given R_{th}, ε.
Output: Optimized active precoding beamforming parameters $\mathbf{W}$;
Optimized passive precoding beamforming parameters Θ and R_s.
(1) Initialize $\mathbf{W}$ and Θ;
(2) **while** no convergence of R_s do;
(3) Convert C1⇔C1′ according to formulation (27);
(4) Update ζ according to (20);
(5) Update η according to (33);
(6) Update $\mathbf{W}$ by solving (37);
(7) Update λ according to (43);
(8) Update Θ by solving (52);
(9) **end while**
(10) return $\mathbf{W}^{opt}$, Θ^{opt} and R_s.

Algorithm 1: Proposed joint precoding algorithm.

malicious signal interference from the jammer. We set up 4 antennas per AP and for the jammer, 2 antennas per user and for the Eve, and 100 reflective elements for the IRS. In Figure 3, "L" represents the distance between the center of the circle where the user is located and the origin. "R" represents the radius of the circle where the users are distributed. Other specific simulation parameters are given in Table 1.

For the channel model, we refer to the setting in reference [9]. We define d_{AR} and d_{JR} as the distances from an AP and the jammer, respectively, to the IRS. d_{AU} and d_{JU} denote the distances from an AP and the jammer, respectively, to a user. d_{AE} denotes the distance from an AP to the Eve. d_{RU} and d_{RE} denote the distances from the IRS to a user and the Eve. For large-scale fading, we adopt a distance-dependent path loss model:

$$L(d) = L_0\left(\frac{d}{d_0}\right)^{-\delta}, d \in \left\{d_{AR}, d_{JR}, d_{AU}, d_{AE}, d_{JU}, d_{RU}, d_{RE}\right\}, \tag{53}$$

where $L_0 = -40$ dB denotes the path loss at a reference distance of $d_0 = 1m$, d denotes the link distance, and δ represents the path loss exponent [41]. For small-scale fading, we consider the Rice fading channel model, using as an example the channel between an AP and user k:

$$\mathbf{H} = L(d_{AU})\left(\sqrt{\frac{\kappa_{AU}}{1+\kappa_{AU}}}\mathbf{H}^{LoS} + \sqrt{\frac{1}{1+\kappa_{AU}}}\mathbf{H}^{NLoS}\right), \tag{54}$$

where κ_{AU} represents the Rician factor and $\mathbf{H}^{LoS}$ and $\mathbf{H}^{NLoS}$ denote line-of-sight (LoS) and nonline-of-sight (NLoS) channels, respectively. Each of the other channels can be generated in a manner similar to equation (54).

Figure 4 shows the weighted sum rate versus the maximum AP transmit power. Here, the CSI uncertainty is $\varepsilon_{m,Eve} = 0.01$, $\varepsilon_{j,i} = 0.01$, and $N = 100$. For a given transmit power, the performance of the proposed algorithm against jamming and eavesdropping is close to the ideal case of no jamming. For comparison, we consider random phase shifts of the IRS and a conventional ZF precoding antijamming algorithm without an IRS. The simulation results show that our proposed algorithm can significantly improve the weighted sum rate of the system and that the use of the IRS somewhat improves the resistance to jamming and eavesdropping and increases the secrecy rate of the system.

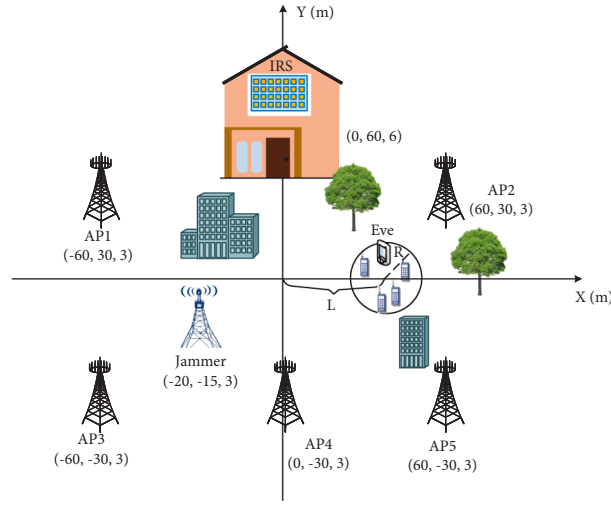

Figure 3: Diagram of the simulation scenario.

Table 1: List of key notations.

Parameter	Value
Bandwidth	180 MHz
Locations of AP1 and AP2	(−60, 30, 3), (60, 30, 3)
Locations of AP3–AP5	(−60, −30, 3), (0, −30, 3), (60, −30, 3)
Location of the jammer	(−20, −15, 3)
$P_{m,\max}$	0 dBm
$P_{J,\max}$	30 dBm
Noise power of user/eve	−80 dBm
Path loss (AP/jammer–IRS)	$\delta_{AR} = \delta_{JR} = 2.2$
Path loss (AP–user/eve)	$\delta_{AU} = \delta_{AE} = 3.5$
Path loss (IRS–user/eve)	$\delta_{RU} = \delta_{RE} = 3$
Rician factor (AP/jammer–IRS)	$\kappa_{AR} = \kappa_{JR} = \infty$
Rician factor (AP/IRS–user/eve)	$\kappa_{AU} = \kappa_{AE} = \kappa_{RU} = \kappa_{RE} = 0$
Radius (R)	5 m

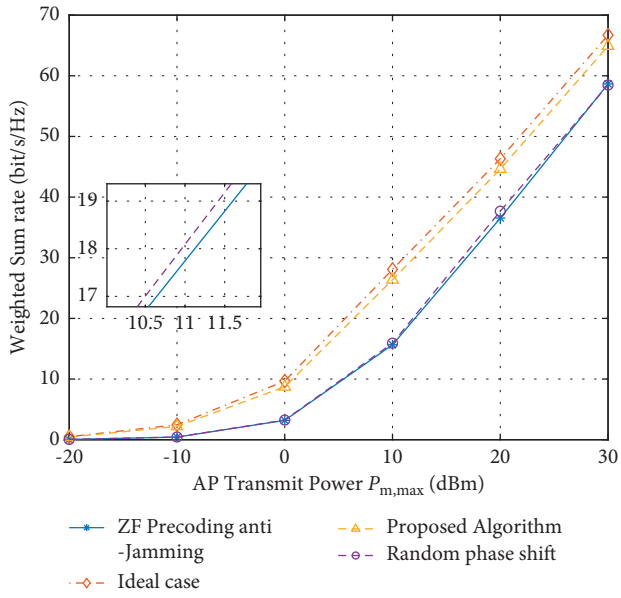

Figure 4: Weighted sum rate versus the AP transmit power $P_{m,\max}$.

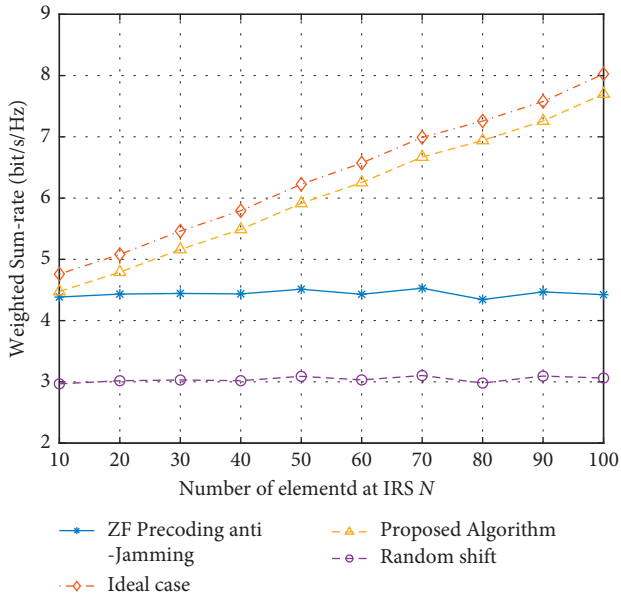

Figure 5: Weighted sum rate versus the number of IRS elements.

Figure 5 shows the weighted sum rate versus the number of IRS elements. We set $\varepsilon_{m,Eve} = 0.01$, $\varepsilon_{j,i} = 0.01$, and $P_{m,\max} = 0$ dBm. We find that both in the ideal case and with our proposed algorithm, the weighted sum rate increases as the number of reflective elements of the IRS increases. The proposed algorithm has a smaller gap relative to the ideal situation without jamming, and increasing the number of IRS elements can effectively improve the performance of the system against jamming and eavesdropping.

Figure 6 shows the weighted sum rate versus the channel estimation error $\varepsilon_{m,Eve}$. We set $P_{m,\max} = 0$ dBm, $\varepsilon_{j,i} = 0.01$, and $N = 100$. From Figure 6, it can be found that in the ideal case without jamming or eavesdropping, the system's sum rate does not vary with the channel estimation error under the assumption that perfect CSI between the APs and legitimate users can be obtained. In contrast, our proposed IRS-enhanced scheme for antijamming and eavesdropping and the conventional ZF precoding antijamming scheme are both affected by the channel estimation error, and the weighted sum rate of the system decreases as the channel estimation error increases; however, our proposed algorithm can still improve the system performance more than the conventional methods in the case of CSI estimation error.

Figure 7 shows the weighted sum rate versus the channel estimation error $\varepsilon_{j,i}$. We set $P_{m,\max} = 0$ dBm, $\varepsilon_{m,Eve} = 0.01$, and $N = 100$. Similar to Figure 6, as the channel estimation

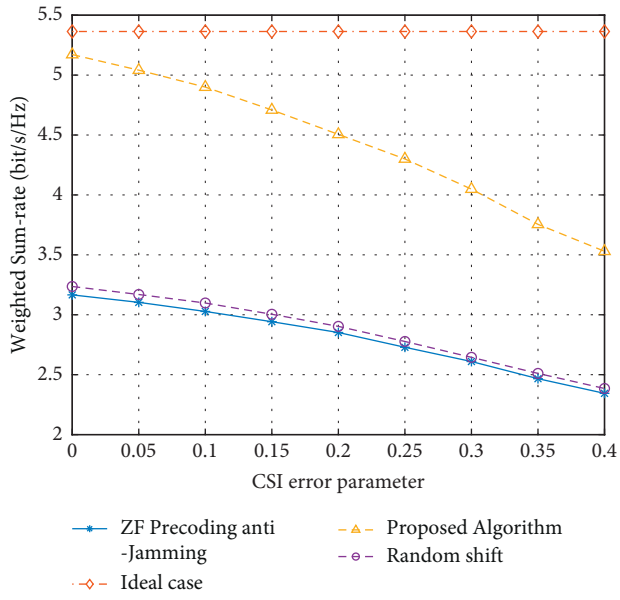

Figure 6: Weighted sum rate versus the CSI error parameter $\varepsilon_{m,Eve}$.

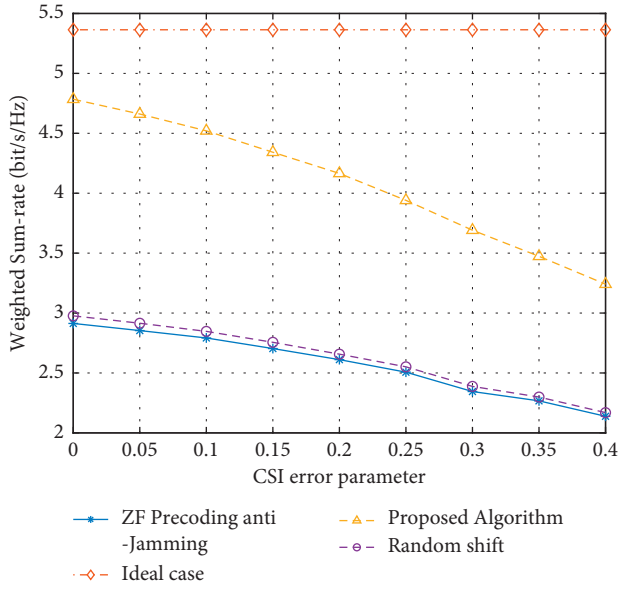

Figure 7: Weighted sum rate versus the CSI error parameter $\varepsilon_{j,i}$.

error $\varepsilon_{j,i}$ increases, the weighted sum rate decreases for all four algorithms in this figure, and the weighted sum rate of the system is lower overall than in Figure 6, which indicates that the channel estimation error $\varepsilon_{j,i}$ of the jammer has a greater impact on the system performance. The reason is that the channel estimation error of the Eve is reflected in the constraint and does not directly affect the sum rate, whereas the jammer directly affects the user SINR; consequently, when $\varepsilon_{j,i}$ increases, the system sum rate will be lower.

Figure 8 shows the weighted sum rate versus the distance travelled by the users (moving from the origin) for the four algorithms. The four curves in this figure exhibit peaks at $L = 60$ and $L = -60$, which coincide with the simulation scenario established in Figure 3. There are two APs at $L = 60$ and $L = -60$. The direct link gain of these two APs plays a major role determining in the sum rate when users move to these two locations. When users move to the location of the jammer, $L = -20$, the interference from the proximity of the jammer causes a significant reduction in the SINR and a sharp drop in the weighted sum rate of the system. When the users move to the IRS location, $L = 0$, the sum rate increases again due to the enhancement of the IRS reflective link. In addition, we observe that the performance of our proposed algorithm is close to the ideal case without jamming, again validating its effectiveness.

We also investigated the convergence performance of the proposed algorithm. Figure 9 shows the weighted sum rate versus the number of iterations for the four algorithms. We

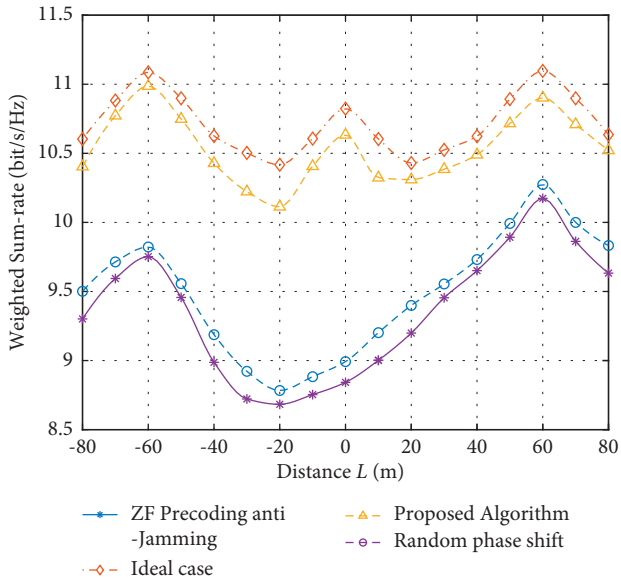

Figure 8: Weighted sum rate versus the distance L.

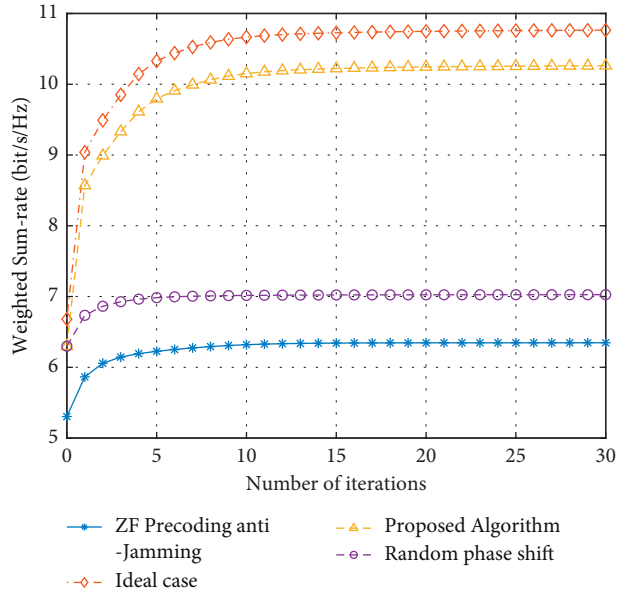

Figure 9: Weighted sum rate versus the number of iterations.

set $P_{m,\max} = 0$ dBm, $\varepsilon_{m,Eve} = 0.01$, $\varepsilon_{j,i} = 0.01$, and $N = 100$. As shown in Figure 9, with an increasing number of iterations, the weighted sum rate reaches a stable value for each of the four algorithms. Our proposed algorithm converges after approximately 10 iterations, and the value is close to that in the ideal case with no jamming, proving the effectiveness of the algorithm. Figure 9 also shows the convergence of the conventional ZF precoding antijamming algorithm and random phase shifts of the IRS; although both algorithms can converge relatively quickly, the stable weighted sum rate obtained is significantly lower than that achieved with our proposed algorithm. Thus, our proposed algorithm yields a clearly superior outcome within an acceptable number of iterations.

6. Conclusion

In this paper, we introduce an IRS into a cell-free massive MIMO network to build an IRS-assisted cell-free massive MIMO antijamming and eavesdropping framework, taking

advantage of the strong antijamming capabilities of cell-free massive MIMO and the low power consumption and flexible deployment of IRSs. Considering imperfect CSI of the Eve and jammer, we investigate the design of an active–passive beamforming scheme for secure IRS-assisted cell-free massive MIMO transmission. We first transform the information leakage constraint into a processable linear matrix inequality by employing the generalized S-procedure and then construct a joint optimization framework under imperfect CSI; transform the multivariate coupled nonconvex problem into a convex optimization problem using FP, MCQT, and other methods; and finally solve for the optimal AP precoding and IRS phase-shift matrices. Simulation results show that our proposed scheme can yield a higher system sum rate than the conventional massive MIMO antijamming methods, thereby verifying the great potential of the proposed scheme for enhancing secure transmission in wireless communications.

Appendix

Proof of Proposition 1. According to Sylvester's determinant identity, $\det(\mathbf{I}+\mathbf{AB})=\det(\mathbf{I}+\mathbf{BA})$, C1 in equation (22) is equivalent to

$$
\begin{aligned}
&\log_2\det\left(\mathbf{I}_U+\left(\sum_{b=1,b\neq k}^{K}\mathbf{F}_{Eve}^H\mathbf{w}_b\mathbf{w}_b^H\mathbf{F}_{Eve}+\sigma_{Eve}^2\mathbf{I}_U\right)^{-1}\times\mathbf{F}_{Eve}^H\mathbf{w}_k\mathbf{w}_k^H\mathbf{F}_{Eve}\right)\leqslant R_{th},\\
&\Leftrightarrow\log_2\left(1+\mathbf{w}_k^H\mathbf{F}_{Eve}\left(\sum_{b=1,b\neq k}^{K}\mathbf{F}_{Eve}^H\mathbf{w}_b\mathbf{w}_b^H\mathbf{F}_{Eve}+\sigma_{Eve}^2\mathbf{I}_U\right)^{-1}\times\mathbf{F}_{Eve}^H\mathbf{w}_k\right)\leqslant R_{th},\\
&\Leftrightarrow\mathrm{Tr}\left(\left(\sum_{b=1,b\neq k}^{K}\mathbf{F}_{Eve}^H\mathbf{w}_b\mathbf{w}_b^H\mathbf{F}_{Eve}+\sigma_{Eve}^2\mathbf{I}_U\right)^{-1}\times\mathbf{F}_{Eve}^H\mathbf{w}_k\mathbf{w}_k^H\mathbf{F}_{Eve}\right)\leqslant 2^{R_{th}}-1,\\
&\Leftrightarrow\lambda_{\max}\left(\left(\sum_{b=1,b\neq k}^{K}\mathbf{F}_{Eve}^H\mathbf{w}_b\mathbf{w}_b^H\mathbf{F}_{Eve}+\sigma_{Eve}^2\mathbf{I}_U\right)^{-1/2}\leqslant\mathbf{F}_{Eve}^H\mathbf{w}_k\mathbf{w}_k^H\mathbf{F}_{Eve}\left(\sum_{b=1,b\neq k}^{K}\mathbf{F}_{Eve}^H\mathbf{w}_b\mathbf{w}_b^H\mathbf{F}_{Eve}+\sigma_{Eve}^2\mathbf{I}_U\right)^{-1/2}\right)\leqslant 2^{R_{th}}-1,\\
&\Leftrightarrow\left(2^{R_{th}}-1\right)\left(\sum_{b=1,b\neq k}^{K}\mathbf{F}_{Eve}^H\mathbf{w}_b\mathbf{w}_b^H\mathbf{F}_{Eve}+\sigma_{Eve}^2\mathbf{I}_U\right)-\mathbf{F}_{Eve}^H\mathbf{w}_k\mathbf{w}_k^H\mathbf{F}_{Eve}\succcurlyeq 0.
\end{aligned}
\tag{A.1}
$$

This concludes the proof of Proposition 1. □

Data Availability

No data were used to support this study.

Conflicts of Interest

The authors declare that they have no conflicts of interest.

Acknowledgments

This work was supported in part by the National Natural Science Foundation of China under Grant nos. 62071485, 61901519, and 62001513 and in part by the Basic Research Project of Jiangsu Province under Grant BK 20192002 and the Natural Science Foundation of Jiangsu Province under Grant BK 20201334 and BK 20200579.

References

[1] J. Hoydis, S. ten Brink, and M. Debbah, "Massive MIMO in the UL/DL of cellular networks: How many antennas do we need?" *IEEE Journal on Selected Areas in Communications*, vol. 31, no. 2, pp. 160–171, 2013.

[2] H. Q. Hien Quoc Ngo, E. G. Larsson, and T. L. Marzetta, "Energy and spectral efficiency of very large multiuser MIMO systems," *IEEE Transactions on Communications*, vol. 61, no. 4, pp. 1436–1449, 2013.

[3] F. Rusek, D. Persson, B. K. Buon Kiong Lau, E. G. Larsson, T. L. Marzetta, and F. Tufvesson, "Scaling up MIMO: Opportunities and challenges with very large arrays," *IEEE Signal Processing Magazine*, vol. 30, no. 1, pp. 40–60, 2013.

[4] A. Abdallah and M. M. Mansour, "Efficient Angle-domain processing for FDD-based cell-free massive MIMO systems," *IEEE Transactions on Communications*, vol. 68, no. 4, pp. 2188–2203, 2020.

[5] Ö. T. Demir, E. Björnson, and L. Sanguinetti, "Foundations of user-Centric cell-free massive MIMO," *Foundations and Trends in Signal Processing*, vol. 14, no. 3-4, pp. 162–472, 2021.

[6] C. Huang, A. Zappone, G. C. Alexandropoulos, M. Debbah, and C. Yuen, "Reconfigurable intelligent surfaces for energy efficiency in wireless communication," *IEEE Transactions on Wireless Communications*, vol. 18, no. 8, pp. 4157–4170, 2019.

[7] E. Basar, M. Di Renzo, J. De Rosny, M. Debbah, M.-S. Alouini, and R. Zhang, "Wireless communications through reconfigurable intelligent surfaces," *IEEE Access*, vol. 7, pp. 116753–116773, 2019.

[8] Q. Wu, S. Zhang, B. Zheng, C. You, and R. Zhang, "Intelligent reflecting surface-aided wireless communications: a Tutorial," *IEEE Transactions on Communications*, vol. 69, no. 5, pp. 3313–3351, 2021.

[9] Q. Wu and R. Zhang, "Intelligent reflecting surface enhanced wireless network via joint active and passive beamforming,"

IEEE Transactions on Wireless Communications, vol. 18, no. 11, pp. 5394–5409, 2019.

[10] K. Ntontin, K. Song, J. Danufane et al., "Reconfigurable intelligent surfaces vs. Relaying: Differences, Similarities, and performance comparison," *IEEE Open Journal of the Communications Society*, vol. 1, pp. 798–807, 2020.

[11] T. Zhou, K. Xu, X. Xia, W. Xie, and X. Yang, "Achievable rate maximization for aerial intelligent reflecting surface-aided cell-free massive MIMO system," in *Proceedings of the IEEE 6th International Conference on Computer and Communications (ICCC)*, pp. 623–628, IEEE, Chengdu, China, December 2020.

[12] C. Huang, A. Zappone, M. Debbah, and C. Yuen, "Achievable rate maximization by passive intelligent mirrors," in *Proceedings of the 2018 IEEE International Conference on Acoustics, Speech and Signal Processing (ICASSP)*, pp. 3714–3718, IEEE, Calgary, AB, Canada, April 2018.

[13] P. Wang, J. Fang, X. Yuan, Z. Chen, and H. Li, "Intelligent reflecting surface-assisted millimeter wave communications: joint active and passive precoding design," *IEEE Transactions on Vehicular Technology*, vol. 69, no. 12, pp. 14960–14973, 2020.

[14] C. Pan, H. Ren, K. Wang et al., "Multicell MIMO communications relying on intelligent reflecting surfaces," *IEEE Transactions on Wireless Communications*, vol. 19, no. 8, pp. 5218–5233, 2020.

[15] Q. Wu and R. Zhang, "Beamforming optimization for wireless network aided by intelligent reflecting surface with discrete phase shifts," *IEEE Transactions on Communications*, vol. 68, no. 3, pp. 1838–1851, 2020.

[16] Q.-U.-A. Nadeem, A. Kammoun, A. Chaaban, M. Debbah, and M.-S. Alouini, "Asymptotic max-min SINR analysis of reconfigurable intelligent surface assisted MISO systems," *IEEE Transactions on Wireless Communications*, vol. 19, no. 12, pp. 7748–7764, 2020.

[17] Z. Zhang and L. Dai, "Capacity Improvement in Wideband reconfigurable intelligent surface-aided cell-free network," in *Proceedings of the 2020 IEEE 21st International Workshop on Signal Processing Advances in Wireless Communications (SPAWC), Atlanta, GA, USA*, pp. 1–5, 2020.

[18] J. Zhu, R. Schober, and V. K. Bhargava, "Linear precoding of data and artificial noise in secure massive MIMO systems," *IEEE Transactions on Wireless Communications*, vol. 15, no. 3, pp. 2245–2261, 2016.

[19] J. Zhu, D. W. K. Ng, N. Wang, R. Bhargava, and V. K. au, "Analysis and design of secure massive MIMO systems in the presence of hardware Impairments," *IEEE Transactions on Wireless Communications*, vol. 16, no. 3, pp. 2001–2016, 2017.

[20] X. Yu, D. Xu, and R. Schober, "Enabling secure wireless communications via intelligent reflecting surfaces," in *Proceedings of the 2019 IEEE Global Communications Conference (GLOBECOM)*, pp. 1–6, IEEE, Waikoloa, HI, USA, December 2019.

[21] Z. Chu, W. Hao, P. Xiao et al., "Secrecy rate optimization for intelligent reflecting surface assisted MIMO system," *IEEE Transactions on Information Forensics and Security*, vol. 16, pp. 1655–1669, 2021.

[22] Y. Sun, K. An, J. Luo, Y. Zhu, G. Zheng, and S. Chatzinotas, "Intelligent reflecting surface enhanced secure transmission against both jamming and eavesdropping attacks," *IEEE Transactions on Vehicular Technology*, vol. 70, no. 10, pp. 11017–11022, 2021.

[23] J. Qiu, K. Xu, X. Xia et al., "Secure transmission scheme based on Fingerprint positioning in cell-free massive MIMO systems," *IEEE Transactions on Signal and Information Processing over Networks*, vol. 8, pp. 92–105, 2022.

[24] X. Wang, Y. Gao, G. Zhang, and M. Guo, "Security performance analysis of cell-free massive MIMO over spatially correlated Rayleigh fading channels with active spoofing attack," in *Proceedings of the 2020 International Conference on Wireless Communications and Signal Processing (WCSP)*, pp. 540–545, IEEE, Nanjing, China, October 2020.

[25] M. Alageli, A. Ikhlef, F. Alsifiany, M. A. M. Abdullah, G. Chen, and J. Chambers, "Optimal downlink transmission for cell-free SWIPT massive MIMO systems with active eavesdropping," *IEEE Transactions on Information Forensics and Security*, vol. 15, pp. 1983–1998, 2020.

[26] X. Zhang, D. Guo, K. An, Z. Ding, and B. Zhang, "Secrecy analysis and active pilot spoofing attack detection for Multigroup Multicasting cell-free massive MIMO systems," *IEEE Access*, vol. 7, pp. 57332–57340, 2019.

[27] S. Elhoushy, M. Ibrahim, and W. Hamouda, "Exploiting RIS for limiting information leakage to active eavesdropper in cell-free massive MIMO," *IEEE Wireless Communications Letters*, vol. 11, no. 3, pp. 443–447, 2022.

[28] S. Asaad, Y. Wu, A. Bereyhi, R. R. Müller, R. F. Schaefer, and H. V. Poor, "Secure active and passive beamforming in IRS-aided MIMO systems," *IEEE Transactions on Information Forensics and Security*, vol. 17, pp. 1300–1315, 2022.

[29] Y. Han, S. Zhang, L. Duan, and R. Zhang, "Cooperative double-IRS aided communication: beamforming design and power scaling," *IEEE Wireless Communications Letters*, vol. 9, no. 8, pp. 1206–1210, 2020.

[30] Z. Zhang and L. Dai, "A joint precoding framework for Wideband reconfigurable intelligent surface-aided cell-free network," *IEEE Transactions on Signal Processing*, vol. 69, pp. 4085–4101, 2021.

[31] J. Chen, X. Chen, W. H. Gerstacker, and D. W. K. Ng, "Resource allocation for a massive MIMO relay aided secure communication," *IEEE Transactions on Information Forensics and Security*, vol. 11, no. 8, pp. 1700–1711, 2016.

[32] D. W. K. Ng, E. S. Lo, and R. Schober, "Robust beamforming for secure communication in systems with wireless information and power transfer," *IEEE Transactions on Wireless Communications*, vol. 13, no. 8, pp. 4599–4615, 2014.

[33] G. Zheng, K.-K. Wong, and T.-S. Ng, "Robust linear MIMO in the down-link: a worst-case optimization with ellipsoidal uncertainty regions," *EURASIP Journal on Applied Signal Processing*, vol. 2008, no. 1, pp. 1–15, 2008.

[34] J. Jiaheng Wang and D. P. Palomar, "Worst-case robust MIMO transmission with imperfect channel knowledge," *IEEE Transactions on Signal Processing*, vol. 57, no. 8, pp. 3086–3100, 2009.

[35] D. Xu, X. Yu, Y. Sun, D. W. K. Ng, and R. Schober, "Resource allocation for IRS-assisted full-duplex cognitive radio systems," 2020, http://arxiv.org/abs/2003.07467.

[36] C. You, B. Zheng, and R. Zhang, "Intelligent reflecting surface with discrete phase shifts: channel estimation and passive beamforming," 2019, http://arxiv.org/abs/1911.03916.

[37] G. Interdonato, E. Björnson, H. Quoc Ngo, P. Frenger, and E. G. Larsson, "Ubiquitous cell-free massive MIMO

communications," *EURASIP Journal on Wireless Communications and Networking*, vol. 2019, no. 1, p. 197, 2019.

[38] K. Shen and W. Yu, "Fractional programming for communication systems-Part I: power control and beamforming," *IEEE Transactions on Signal Processing*, vol. 66, no. 10, pp. 2616–2630, 2018.

[39] Z.-Q. Luo, S. Zhang, and J. F. Sturm, "Multivariate Nonnegative quadratic Mappings," *SSRN Electronic Journal*, vol. 14, no. 4, pp. 1140–1162, 2003.

[40] H. Guo, Y.-C. Liang, J. Chen, and E. G. Larsson, "Weighted sum-rate maximization for reconfigurable intelligent surface aided wireless networks," *IEEE Transactions on Wireless Communications*, vol. 19, no. 5, pp. 3064–3076, 2020.

[41] S. Boyd, N. Parikh, E. Chu, B. Peleato, and J. Eckstein, "Distributed optimization and statistical learning via the alternating direction method of multipliers," *Foundations and Trends in Machine Learning Foundations and Trends® in Machine Learning*, vol. 3, no. 1, pp. 1–122, 2010.

[42] M. Cui, G. Zhang, and R. Zhang, "Secure wireless communication via intelligent reflecting surface," *IEEE Wireless Communications Letters*, vol. 8, no. 5, pp. 1410–1414, 2019.